

# Two dimensional bispectral estimates from ocean SAR images

J. M. Le Caillec, R. Garello<sup>1</sup>

B. Chapron<sup>2</sup>

<sup>1</sup>Félécom Bretagne Dept ITI, BP 832 .29285 Brest Cedex, France

<sup>2</sup>IFREMER, DRO/OS, BP 70, Plouzané, France

Received 29 January 1996 - Revised 13 May 1996 - Accepted 17 July 1996 - Communicated by A. D. Kirwan

**Abstract.** Synthetic Aperture Radar (SAR) images of the ocean yield a lot of information on the sea-state surface providing that the mapping process between the surface and the image is clearly defined. However it is well known that SAR images exhibit non-gaussian statistics and that the motion of the scatterers on the surface, while the image is being formed, may yield to nonlinearities.

The detection and quantification of these nonlinearities are made possible by using Higher Order Spectra (HOS) methods and more specifically, bispectrum estimation. The development of the latter method allowed us to find phase relations between different parts of the image and to recognise their level of coupling, i.e. if and how waves of different wavelengths interacted nonlinearly. This information is quite important as the usual models assume strong nonlinearities when the waves are propagating in the azimuthal direction (i.e. along the satellite track) and almost no nonlinearities when propagating in the range direction. In this paper, the mapping of the ocean surface to the SAR image is reinterpreted and a specific model (i.e. a Second Order Volterra Model) is introduced. The nonlinearities are thus explained as either produced by a nonlinear system or due to waves propagating into selected directions (azimuth or range) and interacting during image formation.

It is shown that quadratic nonlinearities occur for waves propagating near the range direction while for those travelling in the azimuthal direction the nonlinearities, when present, are mostly due to wave interactions but are almost completely removed by the filtering effect coming from the surface motion itself (azimuth cut-off). An inherent quadratic interaction filtering (azimuth high pass filter) is also present. But some other effects, apparently nonlinear, are not detected with the methods described here, meaning that either the usual relation

developed for the Ocean-to-SAR transform is somewhat incomplete, although the mechanisms leading to its formulation seem to be correct, or that these nonlinearities cannot be detected in the classical bispectrum theory.

## 1 Introduction

Imaging of the ocean by satellite-borne SAR (Synthetic Aperture Radar) has been the subject of a large amount of literature for almost the last 20 years now, since the launch of SEASAT in 1978 and more recently of the ERS (European Remote Sensing) satellites series. Special interest has been devoted to the imaging of the ocean surface and one of the main fields of investigation has been the description of the ocean surface mapping to a SAR image (Keller and Wright, 1975; Hasselmann et al., 1985; Alpers and Bruning, 1986; Bruning et al., 1988, 1990; Hasselmann and Hasselmann, 1991; Krogstad, 1992; Krogstad et al., 1994; Hara and Plant, 1994).

The goal pursued by many researchers was to find a SAR spectrum inversion scheme in order to get all the relevant information from a sea spectrum. Many models were developed, especially for taking into account the nonlinear relationship involved in the mapping and due to the motion of the ocean waves during the aperture time (e.g. Alpers et al., 1981; Hasselmann and Hasselmann, 1991).

On the other hand, research in signal processing has been focused, for a long time, on spectrum estimation and information extraction using either non-parametric or parametric methods. However in the last decade, spectrum limitations and especially its phase blindness have involved the development of Higher Order Spectra (HOS) methods (Nikias and Mendel, 1993; Nikias and Petropulu, 1993). Phase estimation is paramount in nonlinear system identification and detection of nonlinearities in one or two dimensional (1D or 2D) signals.

It thus seemed then natural to apply these new tools to the case of SAR images where nonlinearities may happen, according to the theory, and try to find their location and understand why they were present in order to give a better insight into the SAR inversion problem.

In this paper our main purpose is to detect and quantify the nonlinearities in SAR images. For that reason, the bispectrum estimation methods had to be developed and adapted to the 2D case. Indeed, this kind of analysis is seldom encountered for images as there is a rather large amount of calculations which consume lots of memory consuming.

Firstly, we had to analyse the SAR transform and to simplify the problem, we retained the prominent models (e.g. Hasselmann and Hasselmann, 1991), that are currently widely accepted. These models are divided into two parts : a linear part, describing the direct mapping of the ocean without motion (RAR, or Real Aperture Radar transform) followed by a part due to the motion (denoted the RAR to SAR transform) and presenting all the nonlinearities. Our goal is thus to detect the nonlinearities occurring for the whole mapping without considering a two step transform.

Furthermore, many authors have explained the possible nonlinearities by considering the waves travelling in the azimuth (along track) or range (across track) directions and setting some level of nonlinearities in the former case. In order to verify if our analysis was relevant we simulated a nonlinear image by mixing the two parts described above, in parallel ways (linear and quadratic) using a Second Order Volterra Model. We then applied our method to the case of real SAR images acquired from the ERS-1 satellite and we selected images showing three cases of travelling waves : range, azimuth and in-between.

The first section presents the background for SAR imaging theory and HOS definitions. It is then followed by a section on 2D signal bispectrum (or its normalised version, bicoherence) estimation where a solution for visualising and analysing the information contained in a four dimensional support is provided. Finally results and interpretation are given for the simulated images and the real ERS-1 ocean surface images. The methods developed give us an insight into understanding the mechanisms involved in the arising of nonlinearities in the particular case of the analysis of ocean SAR images.

## 2 Theoretical background

### 2.1 SAR mapping

The study of ocean surface mapping by a satellite-borne SAR, and corollary the SAR spectrum inversion have been the subject of abundant literature (Alpers and Bruning, 1986; Bruning et al., 1988; Hasselmann and Hasselmann, 1991; Krogstad, 1992). We assume that

an ocean surface can be seen as generated by the sum of independent oscillators of wavelength  $k$  and pulsation  $\omega$  (Hasselmann and Hasselmann, 1991), which provides the following wave height  $\zeta(r, t)$  expression,

$$\zeta(r, t) = \sum_k \zeta_k e^{j\varphi_k} \cdot e^{j(k \cdot r - \omega \cdot t)} + \text{complex conjugate} \quad (1)$$

with  $\omega = (g \cdot |k|)^{\frac{1}{2}}$  and  $k = (k_x, k_y)$  (in this paper all variables, except on contrary indications, will be 2D arrays). The Fourier coefficient is divided into its magnitude  $\zeta_k$  (which is a real nonnegative value) and its phase  $\varphi_k$ . We admit that the  $\varphi_k$  are uniformly distributed over  $[0, 2\pi]$  and are independent for each wavelength. Consequently the sea spectrum  $S_{sea}(k)$  is given by:

$$S_{sea}(k) \cdot (\Delta k)^2 = \{\zeta_k \cdot e^{j \cdot \varphi_k} \cdot \zeta_k \cdot e^{-j \cdot \varphi_k}\} = E\{\zeta_k^2\} \\ \text{and} \quad E\{\zeta_{k_1} \cdot e^{j \cdot \varphi_{k_1}} \cdot \zeta_{k_2} \cdot e^{-j \cdot \varphi_{k_2}}\} = 0 \quad (2)$$

where  $E\{\}$  denotes the mathematical expectation and  $\Delta k$  is the step width of the wave vector. However, this assumption does not imply that  $E\{\zeta_{k_1} \cdot \zeta_{k_2}\} = 0$ . The RAR image amplitude field is given by:

$$\sigma(r, t) = \bar{\sigma} \left( 1 + \sum_k m_k \cdot e^{j(k \cdot r - \omega \cdot t)} + \text{complex conjugate} \right) \quad (3)$$

where  $\sigma(r, t)$  denotes the radar backscattering cross section and  $\bar{\sigma}$  its spatial mean,  $m_k$  is then a complex value. As previously said, the radar backscattering cross section is linearly related to the wave amplitude  $\zeta_k$ .

$$m_k = T_k \cdot \zeta_k \cdot e^{j\varphi_k} \quad (4)$$

The RAR linear transfer function  $T_k$  is the sum of three successive Modulation Transfer Functions (MTFs). The first one takes into account the fact that SAR images are built up in consecutive strips and so waves can propagate between two successive surface illuminations by the radar and consequently may induce a spectrum rotation (scanning distortion). However, as usual, this distortion is neglected for satellite-borne radar. The "tilt modulation" is due to the angle between the target and the radar beam and depends on the radar characteristics (incident angle, polarisation ...) (Hasselmann and Hasselmann, 1991). The "hydrodynamic modulation", the lesser known of the MTF, takes into account the energy transfer between short waves and long waves and can play a significant role since the Bragg scattering model is valid at the considered incident angle (e.g. Keller and Wright, 1975; Hara and Plant, 1994). However, this theoretical model is not always well verified and even the assumption of a linear hydrodynamic modulation (and consequently of a linear RAR modulation) must be examined more carefully.

The nonlinear step is due to wave motion during the

illumination. In the non dispersive theory, the radar backscattering cross section is misplaced in the azimuth direction, and so an SAR pixel is the sum of different RAR pixels (as usual, the range direction, i.e. the perpendicular direction to the satellite track, is in the y-axis and the azimuth direction, i.e. along the satellite path, is in the x-axis). Because the misplacement is proportional to the wave orbital velocity in the range direction and the radar backscattering cross section is alternatively bunched and dilated, this phenomenon is called the "velocity bunching". Such a phenomenon is a constructive mechanism and implies strong nonlinearities especially when waves propagate along the satellite track. Under a gaussian statistical description of the displacement field, the SAR image spectrum expression has been derived, and is linked both with the misplacement and the RAR image spectrum. The SAR Fourier coefficient  $\tilde{X}^{sar}(k)$  can be easily expressed using a summation over the RAR pixels  $I^{rar}(x)$  by:

$$\tilde{X}^{sar}(k) = \int_A I^{rar}(x) \cdot e^{jk_x \cdot \epsilon(x)} \cdot e^{-j \cdot k \cdot x} \cdot dx \quad (5)$$

where  $A$  is a given surface of summation and  $\epsilon(x)$  the misplacement. Under gaussian statistics of the sea surface, and when  $A \rightarrow \infty$  we obtain the following SAR spectrum:

$$S_{sar}(k) = I_o^2 \cdot \int_x e^{-j \cdot k \cdot x} \cdot e^{-k_x^2 \cdot (\rho_{\epsilon\epsilon}(0) - \rho_{\epsilon\epsilon}(x))} \cdot (1 + \rho_{II}(x) + j \cdot k_x \cdot (\rho_{I\epsilon}(x) - \rho_{I\epsilon}(-x)) + k_x^2 \cdot (\rho_{I\epsilon}(0) - \rho_{I\epsilon}(x)) \cdot (\rho_{I\epsilon}(0) - \rho_{I\epsilon}(-x))) \cdot dx \quad (6)$$

where  $\rho$  denotes the correlation function. Because the RAR image and the displacement field are linearly derived from the Discrete Fourier Transform (DFT) coefficients of the sea surface, the nonlinearity is due to the exponential term. Krogstad in Krogstad et al. (1994) noticed that, by expanding the exponential of (6) and by taking a modulated Gaussian distribution for the displacement field correlation function, each order of the expansion can be seen as a higher order harmonic spectrum (smaller and smaller as the order increases). Another degradation caused by the wave motion is the azimuth smearing which induces an azimuth resolution decrease and is related to the orbital acceleration and the orbital velocity spread within a resolution cell. This degradation is explicitly contained in the term  $e^{-k_x^2 \cdot (\rho_{\epsilon\epsilon}(0))}$  in (6). For further information on the SAR imaging process a good bibliography may be found in Hasselmann and Hasselmann (1991).

## 2.2 Higher order spectra definitions and properties.

The third order moment, for a 2D signal  $X(i)$ , is defined (Nikias and Raghuveer, 1987; Giannakis and Swami,

1988; Nikias and Mendel, 1993; Nikias and Petropulu, 1993) by:

$$M_3^X(n_1, n_2) = E\{X(i) \cdot X(i + n_1) \cdot X(i + n_2)\} \quad (7)$$

with  $n_1 = (n_x^1, n_y^1)$ . This definition implies the same six symmetry relations as for one dimensional signals:

$$\begin{aligned} M_3^X(n_1, n_2) &= M_3^X(n_2, n_1) = M_3^X(n_2 - n_1, -n_1) = \\ M_3^X(-n_1, n_2 - n_1) &= M_3^X(n_1 - n_2, -n_2) \\ &= M_3^X(-n_2, n_1 - n_2) \end{aligned} \quad (8)$$

Two equivalent bispectrum definitions can be formulated. First, the bispectrum is the four dimensional Fourier Transform of the third order moment:

$$B(k_1, k_2) = \sum_{n_1=-\infty}^{+\infty} \sum_{n_2=-\infty}^{+\infty} M_3^X(n_1, n_2) e^{-j(k_1 \cdot n_1 + k_2 \cdot n_2)} \quad (9)$$

( $\sum_{n_1, n_2=-\infty}^{+\infty}$  is a 2D summation). Secondly, it may be expressed by the mathematical expectation of the Fourier coefficient triple product,

$$B(k_1, k_2) = E\{\tilde{X}(k_1) \cdot \tilde{X}(k_2) \cdot \tilde{X}^*(k_1 + k_2)\} \quad (10)$$

where  $\tilde{X}(k) = DFT(X(i))$ . The Fourier Transform changes the third order moment symmetry relations into eleven bispectral symmetry relations very similar to one dimension signal bispectral symmetry relations (Nikias and Mendel, 1993; Nikias and Petropulu, 1993, Chapter 1), the third order moment support and the bispectrum support are depicted in fig.1 and fig.2.

$$\begin{aligned} B(k_1, k_2) &= B^*(-k_1, -k_2) = B(k_2, k_1) = \\ B(-k_1 - k_2, k_2) &= B(-k_1 - k_2, k_1) = \\ B(k_1, -k_1 - k_2) &= B(k_2, -k_1 - k_2) \end{aligned} \quad (11)$$

As mentioned in the introduction, the third order moment is phase sensitive and especially sensitive to phase coupling. If we assume a signal which can be written as

$$\begin{aligned} X(i) &= \cos(k_1 \cdot i + \varphi_1) + \cos(k_2 \cdot i + \varphi_2) \\ &+ \cos((k_1 + k_2) \cdot i + \varphi_1 + \varphi_2) \\ &+ \cos(k_3 \cdot i + \varphi_3) + \cos(k_4 \cdot i + \varphi_4) \\ &+ \cos((k_3 + k_4) \cdot i + \varphi_5) + N(i) \end{aligned} \quad (12)$$

where  $N(i)$  is a gaussian noise and  $\varphi_i$  are random phases distributed over  $[0, 2\pi]$ , then only the quadratically phase coupled signal part  $(k_1, k_2, k_1 + k_2)$  appears in the third order moment, and consequently is detected by the bis-

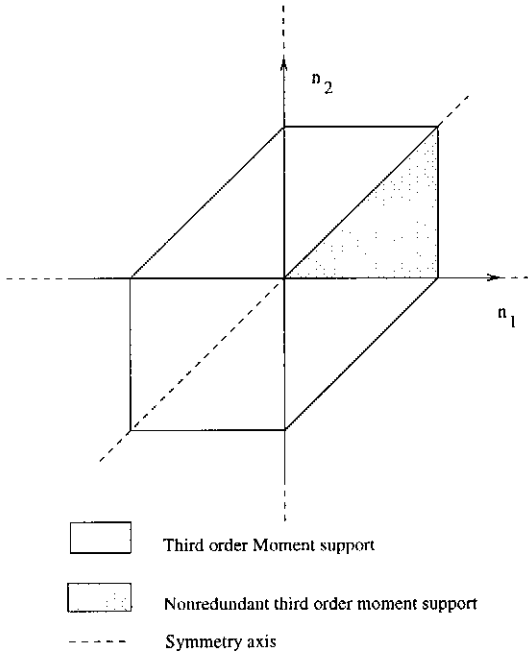


Fig. 1. Third order moment support

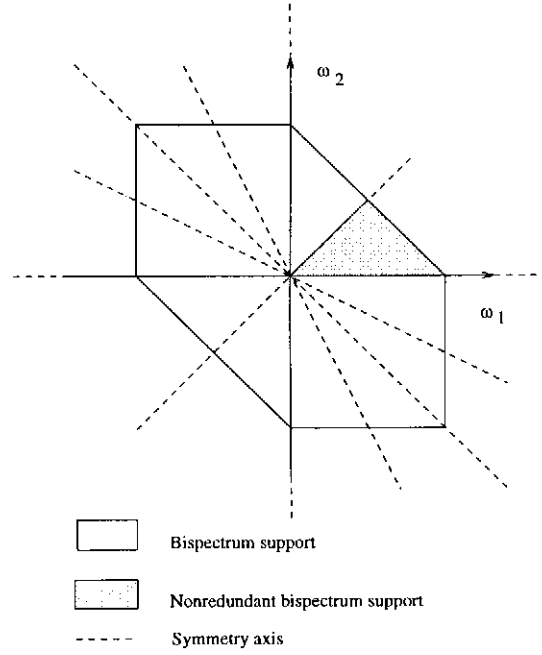


Fig. 2. Bispectrum support

pectrum:

$$\begin{aligned}
 M_3^X(n_1, n_2) = & \frac{1}{4} [\cos(k_2.n_1 - (k_1 + k_2).n_2) \\
 & + \cos(k_2.n_2 - (k_1 + k_2).n_1)) \\
 & + \cos(k_1.n_1 - (k_1 + k_2).n_2) \\
 & + \cos(k_1.n_2 - (k_1 + k_2).n_1) + \cos(k_1.n_1 + k_2.n_2) \\
 & + \cos(k_1.n_1 + k_2.n_2) + \cos(k_1.n_2 + k_2.n_1)] \quad (13)
 \end{aligned}$$

However it must be noted that to estimate the third order moment for detecting phase coupling, several signal trials are needed, a point on which we will elaborate in the next section. A similar calculation can be made in the Fourier domain. The DFT coefficient of (12) is

$$\begin{aligned}
 \tilde{X}(k) = & \frac{1}{2} \cdot (e^{j\varphi_1} \delta(k - k_1) + e^{-j\varphi_1} \delta(k + k_1) \\
 & + e^{j\varphi_2} \delta(k - k_2) + e^{-j\varphi_2} \delta(k + k_2) \\
 & + e^{j(\varphi_1+\varphi_2)} \delta(k - k_1 - k_2) + e^{-j(\varphi_1+\varphi_2)} \delta(k + k_1 + k_2) \\
 & + e^{j\varphi_3} \delta(k - k_3) + e^{-j\varphi_3} \delta(k + k_3) + e^{j\varphi_4} \delta(k - k_4) \\
 & + e^{-j\varphi_4} \delta(k + k_4) + e^{j\varphi_5} \delta(k - k_3 - k_4) \\
 & + e^{-j\varphi_5} \delta(k + k_3 + k_4)) \quad (14)
 \end{aligned}$$

where  $\delta(k)$  denotes the Dirac function. By applying (10), the bispectrum is non null if the phase of the triple product is null. For instance  $e^{j\varphi_1} \cdot e^{j\varphi_2} \cdot e^{-j(\varphi_1+\varphi_2)}$  have a non null mean value because the phase is null, and

then the bispectrum is non null for  $(k_1, k_2)$ . Meanwhile  $e^{j\varphi_3} \cdot e^{j\varphi_4} \cdot e^{-j\varphi_5}$  have a null mean because  $\varphi_3 + \varphi_4 - \varphi_5$  is uniformly distributed over  $[0, 2\pi]$  (and then  $B(k_3, k_4)$  is null). Another important remark is that the three sinusoids are a symmetric triplet, because the sinusoids of pulsation  $k_1$  can be seen as generated by the difference of waves  $k_2, k_1 + k_2$ . The quadratically phase coupling notion is relevant for quadratic nonlinearity detection. As a matter of fact, if we consider the Second Order Volterra Model depicted in fig. 3, sinusoids at the

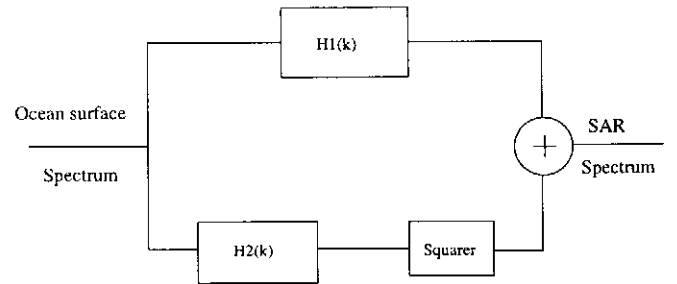


Fig. 3. Second Order Volterra Model

squarer output are quadratically phase coupled with the input ones, and so the linear path output sinusoids and the quadratic path output ones are quadratically phase coupled (except for  $H_1(k)$  and  $H_2(k)$  phase shifts, and for this reason it would be better to say "phase coherent"). This kind of nonlinear model has been widely studied in Schetzen (1980), and applied for nonlinear

wave interactions in plasma (Kim and Powers, 1988, 1979). But for each pair  $(k_1, k_2)$ , energy at the frequency  $k_1 + k_2$ , in the model in fig. 3 is the sum of the energy provided by the linear path and by the quadratic interaction of sinusoids of wavenumber  $k_1$  and  $k_2$ . In order to estimate the energy passing through each part (and so to give a level of nonlinearity), a useful quantity is the bicoherence defined as:

$$P(k_1, k_2) = \frac{B(k_1, k_2)}{\sqrt{S(k_1) \cdot S(k_2) \cdot S(k_1 + k_2)}} \quad (15)$$

where  $S(k)$  is the spectrum. In fact, if:

$$\begin{aligned} X(i) = & A_1 \cdot \cos(k_1 \cdot i + \varphi_1) + A_2 \cdot \cos(k_2 \cdot i + \varphi_2) \\ & + A_3 \cdot \cos((k_1 + k_2) \cdot i + \varphi_1 + \varphi_2) \\ & + B \cdot \cos((k_1 + k_2) \cdot i + \varphi_3) + N(i) \end{aligned} \quad (16)$$

where  $\varphi_i|_{i=1,2,3}$  are random phases, and since the third order moment is only sensitive to phase coupling, then the bicoherence is equal to:

$$P(k_1, k_2) = \frac{A_3}{\sqrt{(A_3)^2 + B^2}} \quad (17)$$

So the bicoherence gives an idea of the interaction between two waves in the observed signal. In this case, if the signal is "linear" (i.e. produced by a linear combination of oscillators independent in magnitude and phase), then the bicoherence is null. Contrary to a common idea, the bicoherence can be greater than 1.0 (Raghuvver, 1990). In the more general case, if the signal is assumed to be obtained by a linear combination of a stochastic variable at different lags (and not by a harmonic decomposition) the bicoherence is not equal to 0 but is flat. For instance, nonsymmetric noise driving a linear system has a bicoherence equal to  $\gamma_3/\gamma_2$  ( $\gamma_3$  and  $\gamma_2$  are respectively the third and second order moments of the noise) over all the bifrequency domain. In the case of (16), because the bicoherence flatness is an indication of system linearity, the bicoherence standard deviation is a good nonlinearity estimator, as will be shown in the last section. However several signal trials, with independent phases, are needed to detect phase coupling. But generally only one realisation is available and, as we will see in section 3, the solution is to divide the signal into subsignals assuming the phase independence of the Fourier coefficients, for each realisation.

The Second Order Volterra Model described above can be seen as a special case of nonlinear filters. If we consider a general nonlinear transfer function where the output depends on a finite number of input samples, such as:

$$Y(i) = F(X(i - p^-), \dots, X(i), \dots, X(i + p^+)) \quad (18)$$

where  $p^-, p^+$  are 2D arrays of nonnegative integers and assuming there exists a Taylor expansion of  $F$ , then:

$$\begin{aligned} Y(i) = & F(0, \dots, 0, \dots, 0) + \\ & \sum_{k=p^-}^{p^+} \frac{\partial F(X(i - p^-), \dots, X(i), \dots, X(i + p^+))}{\partial X(i + k)} \cdot X(i + k) \\ & + \sum_{k=p^-}^{p^+} \sum_{k'=p^-}^{p^+} \frac{\partial^2 F(X(i - p^-), \dots, X(i), \dots, X(i + p^+))}{\partial X(i + k) \cdot \partial X(i + k')} \cdot X(i + k) \cdot X(i + k') + \dots \end{aligned} \quad (19)$$

where all partial derivative values are taken at the origin. Thus, such a model is a general nonlinear filter approximation up to the second order. In this approximation, nonlinearities of order higher than two will be included in the linear part due to the blindness of the third order moment to higher order phase coupling (Nikias and Mendel, 1993). One of the main problems involved with Higher Order Statistics remains the estimation of these statistics. In the next section, we present in the next section some 2D signal bispectrum estimators and two conventional ones in particular.

### 3 2D signal bispectrum estimation

Bispectral estimators are divided into two classes in the same way as spectral estimators are, a conventional Fourier-type class and a parametric one (Nikias and Raghuvver, 1987; Nikias and Mendel, 1993; Nikias and Petropulu, 1993, Chapter 4). The conventional class is made up of two classical estimators (direct and indirect methods) based upon both definitions of section 2. The direct method consists in averaging the DFT coefficients over all available signal trials, and possibly a frequency smoothing which decreases the estimation variance. This estimation method has been initially developed for 2D signal in Chandran and Elgar (1990) (without frequency averaging). If it is assumed that the bispectrum is estimated over an  $(N_0)^4$  grid and the odd averaging window size is fixed to  $M_n$ , ( $M_n = 2 \cdot J_n + 1$ ), then the signal data length must be adjusted to  $L = M_n \cdot N_0$ , either by decreasing the signal length or by zero padding. So for the  $n$ th centred signal realisation of finite length  $N^2$ :

$$\hat{B}^n(k_1, k_2) = \sum_{j_1=-J_n}^{+J_n} \sum_{j_2=-J_n}^{+J_n} F(k_1 \cdot M_n + j_1) \cdot F(k_2 \cdot M_n + j_2) \cdot F^*(k_1 + k_2 \cdot M_n + j_1 + j_2) \quad (20)$$

With:

$$F(\lambda) = \frac{1}{L^2} \sum_{i=0}^L X_n(i) \cdot e^{-j \left( \frac{2 \cdot \pi \cdot i \cdot \lambda}{L} \right)} \quad (21)$$

Some direct submethods, not detailed in this paper, are also described in Nikias and Raghuveer (1987); Nikias and Mendel (1993); Nikias and Petropulu (1993), pp 132-147.

The indirect method (Higher Order Correlogram) is simply the finite Fourier Transform of the windowed third order moment:

$$\hat{B}^n(k_1, k_2) = \sum_{n_1=-J_n}^{+J_n} \sum_{n_2=-J_n}^{+J_n} W(n_1, n_2) \cdot \hat{M}_3^{X_n}(n_1, n_2) \cdot e^{-j(k_1 \cdot n_1 + k_2 \cdot n_2)} \quad (22)$$

With:

$$\hat{M}_3^{X_n}(n_1, n_2) = \sum_{i \in S(M)} X_n(i) X_n(i + n_1) X_n(i + n_2) \quad (23)$$

And

$$S(M) = [sup(0, -n_x^1, -n_x^2), inf(N, N - n_x^1, N - n_x^2)] X [sup(0, -n_y^1, -n_y^2), inf(N, N - n_y^1, N - n_y^2)] \quad (24)$$

The four dimensional window is the product by itself of a two dimensional window (Parzen, Optimal ...) used for 1D signal bispectrum estimation,  $W^{2D}(n_1, n_2) = W^{1D}(n_1) \cdot W^{1D}(n_2)$ , (Nikias and Raghuveer, 1987; Nikias and Mendel, 1993; Nikias and Petropulu, 1993, pp 124-132). Furthermore, in all estimations presented below only a simple 4D rectangular window was used.

Finally, for both methods, the bispectrum estimation is computed by averaging all the bispectrum estimations of the different trials,

$$\hat{B}(k_1, k_2) = \frac{1}{M} \sum_{n=1}^M \hat{B}^n(k_1, k_2) \quad (25)$$

where  $M$  denotes the number of realisations. The parametric class uses a linear system identification from third order moment lags and then computes the bispectrum by triple product. However, the bispectrum estimation by triple product does not always seem possible (Erdem and Tekalp, 1992). Some parametric estimators work for bispectrum estimation and phase coupling detection. For instance an AR model identification using Yule-Walker equations generalised to Higher Order Statistics is described in Raghuveer and Nikias (1985). Also, the ARMA model estimation is presented in Giannakis and Swami (1988); Giannakis and Mendel (1990), and an extension to 2D signal is presented in Le Caillec

et al. (1995). But parametric estimators remain very bad quantifiers and their use in nonlinearity detection is troublesome. For these reasons, results presented in the following section are based only upon conventional estimators. The spectrum estimation needed for the bicoherence estimation is also based on classical spectrum estimators. Consequently the bicoherence is estimated using either indirect method and correlogram or direct method and periodogram. An important problem, specific to the 2D signal bispectrum, is the visualisation of information contained in a 4D structure. For this reason we have introduced bicoherence tables as described in the following section.

#### 4 Bicoherence tables (BTs)

In order to summarise in 2D structures the information contained in the bicoherence, we have defined the three following Bicoherence Tables (BTs).

-Range Azimuth (RA) table:

$$T_{RA}(k_x^1, k_y^1) = \sum_{k_x^2} \sum_{k_y^2} \left( P(k_x^1, k_y^1, k_x^2, k_y^2) - C \right)^2 \quad (26)$$

-Range Range (RR) table:

$$T_{RR}(k_y^1, k_y^2) = \sum_{k_x^1} \sum_{k_x^2} \left( P(k_x^1, k_y^1, k_x^2, k_y^2) - C \right)^2 \quad (27)$$

- Azimuth Azimuth (AA) table:

$$T_{AA}(k_x^1, k_x^2) = \sum_{k_y^1} \sum_{k_y^2} \left( P(k_x^1, k_y^1, k_x^2, k_y^2) - C \right)^2 \quad (28)$$

where  $C$  would be the linear filter bicoherence value, which would have been equal to 0 in our signal decomposition assumption if we had dealt with an infinite number of trials. Because this number is finite the bicoherence is not equal to 0 when there is no phase coupling, but has a mean of about 0.20 for sixteen realisations (the number which has been used in our simulations). In order to take into account this relevant problem,  $C$  has been fixed to 0.20 and all bicoherence values under this mean have not been used for BT computation. This issue of the number of realisations is discussed again in the conclusion. What is the "physical" interpretation of these BTs? The RA table gives the amount of interaction of wave  $k_1$  with the other spectrum waves. The RR and AA tables give the interaction between the waves located on the axis  $k_x = k_x^1$  (resp  $k_y = k_y^1$ ) with the waves located along the axis  $k_x = k_x^2$  (resp  $k_y = k_y^2$ ). These tables give the amount of interaction along the coordinates axis and can be seen as 1D signal bicoherence. It must be noted that these BTs do not have the same symmetry relations as the bispectrum (a plane in the bispectrum coordinates is not necessarily transformed

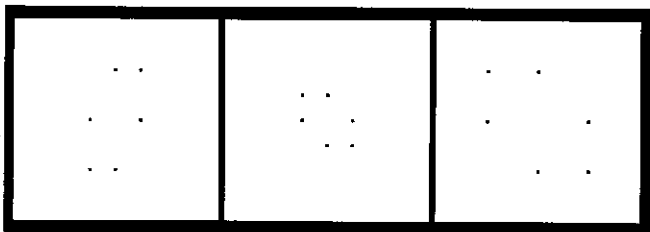


Fig. 4. Phase coupling detection (both methods)

into a parallel plane by symmetry), but some basic relations are always valid. These BTs are a first step to locating nonlinearities, but a finer analysis can only be made with the bicoherence. In order to understand how these BTs work, some examples are related in the next section.

## 5 Results and Discussion

Initially, the bispectrum was estimated over a  $[64]^4$  grid (size due to memory limitations) for both methods. In order to calculate a more accurate estimation for sea surface bispectrum, we computed it over the same number of frequency samples, but using a normalised frequency range equal to  $[-0.25, 0.25]$  instead of  $[-0.5, 0.5]$  (the normalised frequency is usually defined as the real frequency divided by the sampling frequency). For the indirect method, the bispectrum computation on such a support would have needed, a third order moment estimation over  $[128]^4$  lags which is impossible due to memory limitations. So for sea surfaces (simulated or not), only the direct method is available for the time being. For the tests performed on simulated images, sixteen  $[128]X[128]$  independent trials were generated. For ERS-1 images, sixteen  $[128]X[128]$  subsets were taken from the  $[256]X[512]$  imagette (with consequently some overlapping), and were assumed to be independent signal trials (point which we will discuss in the conclusion). In order to avoid incoherent values, only the points where  $\sqrt{S(k_1).S(k_2).S(k_1+k_2)}$  was greater than 10% of the maximum value of this squared root triple product were taken into account to compute the bicoherence.

### 5.1 Simulated 2D Second Order Volterra Models

In this first subsection, three examples are provided. The first one is only made up of waves with phase coupling. The next two examples are the output of a Second Order Volterra model, without filtering in the second example and partial filtering in the third one.

#### First example: Phase coupled sinusoids

The first signal is made up of four waves, the third wave

being phase coupled with the first two and the fourth being without phase coupling, i.e. by taking the notations of (16)  $A_1=A_2=A_3=1$ ,  $B=2$ ,  $k_1=(\pi/2, 0)$ ,  $k_2=(0, \pi/4)$ . BTs are presented (fig. 4) for the whole bispectrum estimation (both methods providing the same results), and we can find non null values, for the plane including the point  $(\pi/2, 0, 0, \pi/4)$ , i.e. the points  $(0, \pi/4)$ ,  $(\pi/2, 0)$ ,  $(\pi/2, \pi/4)$  in the RR table (consequently the perfect symmetry between the three sinusoids is retrieved). Non null values are also found at point  $(\pi/2, 0)$  (resp  $(\pi/4, 0)$ ) and their bispectral symmetric points in the RR table (resp the AA table). For this signal, in order to estimate the bispectrum variance, the bispectrum was estimated from ten different sets of sixteen independent realisations. For the non null bispectrum components, we obtain  $0.254 \pm 0.065$  (the theoretical value is  $2/8 = 0.25$ ). The result is satisfactory but other tests with noisy data remain to be made. In order to well explain how bicoherence, and BTs work we simulated some nonlinear interactions on a more complicated signal.

#### Second example: Complete "nonlinear" signal

In this example, we considered a signal with a finite bandwidth spectrum.

$$\zeta_k = 0 \text{ if } k \notin M = \pm[B_1^x, B_2^x]X[B_1^y, B_2^y] \quad (29)$$

where  $\zeta_k$  is real and nonnegative (as in (1)). We chose in this case a Pierson-Moskowitz spectrum, multiplied by Hasselmann's spreading function introduced in Hasselmann et al. (1985), in order to simulate a sea surface (Mastin et al., 1987). The angle between the wind parameter direction ( $U_{10}$ ) and the range axis is equal to  $45^\circ$  and the wind speed equals  $15 \text{ ms}^{-1}$ . The range resolution was set equal to  $16 \text{ m}$  and the azimuth resolution to  $20 \text{ m}$  (as for ERS-1). The result of the simulated spectrum is reported in fig. 6, and the simulated image (deduced from the squared root spectrum with random phases) is shown in fig. 5. A nonlinear signal was generated from this original signal by squaring it and by multiplying the squared signal by a coefficient  $\alpha$  ( $\alpha = 6.10^{-3}$ ) in order to keep the same order of magnitude for the original and the squared spectra (it is equivalent in fig. 3 to reducing  $H_1(k)$  and  $H_2(k)$  to all-pass filters). The final nonlinear image (fig. 7) results from the sum of the original signal and the multiplied squared signal. Its spectrum (fig. 8) is split into three parts, a medium wavelength spectrum provided by the original signal (in our case about 200 meters)

$$\zeta_k \in M = \pm[B_1^x, B_2^x]X[B_1^y, B_2^y] \quad (30)$$

a long wavelengths spectrum obtained by "destructive" interactions between the waves,

$$\zeta_k^d \in L = [B_1^x - B_2^x, B_2^x - B_1^x]X[B_1^y - B_2^y, B_2^y - B_1^y] \quad (31)$$

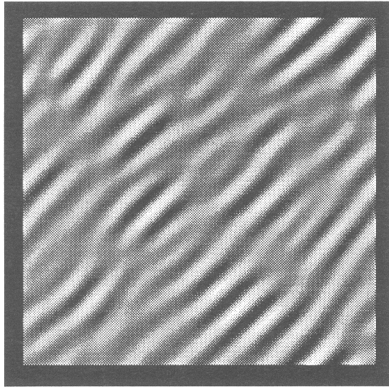


Fig. 5. Original signal

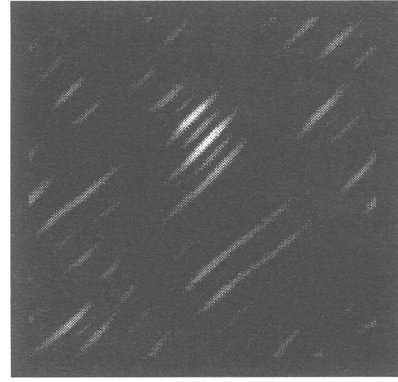


Fig. 7. Final signal

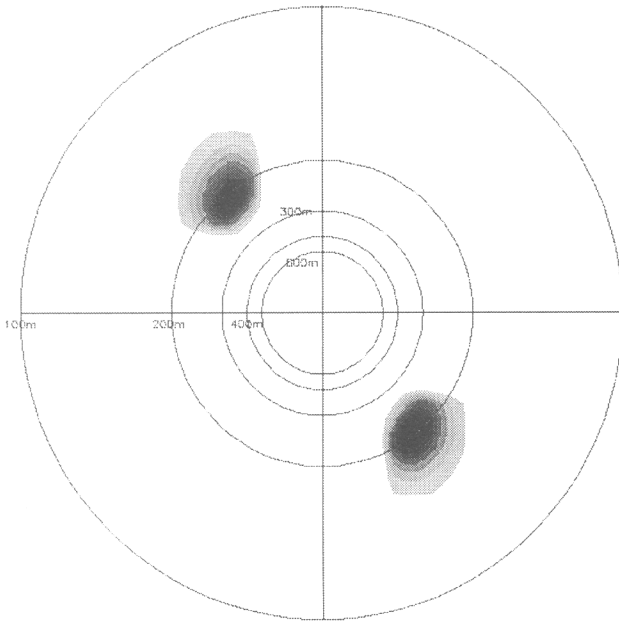


Fig. 6. Original signal spectrum

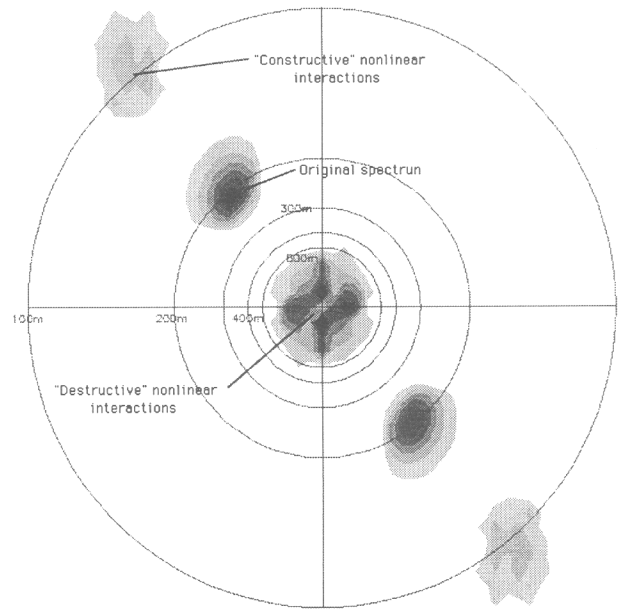


Fig. 8. Final signal spectrum

and a short wavelengths spectrum obtained by "constructive" interactions

$$\zeta_k^{sc} \in S = \pm[2 * B_1^x, 2 * B_2^x]X[2 * B_1^y, 2 * B_2^y] \quad (32)$$

as shown in fig. 8. For short wavelengths, the magnitude expression is equal to

$$\zeta_k^{sc} = \frac{\alpha}{2} \sum_n \zeta_n \cdot \zeta_{k-n} \cdot e^{j(\varphi_n + \varphi_{k-n})} \quad (33)$$

and the spectrum:

$$S(k) \cdot (\Delta k)^2 = E\{\zeta_k^{sc}(\zeta_k^{sc})^*\} = \frac{\alpha^2}{4} \sum_n E\{(\zeta_n \cdot \zeta_{k-n})^2\} \quad (34)$$

( $\sum_n$  in the following of this section denotes the 2D summation over the spectrum bandwidth), and for the long

wavelengths

$$\zeta_k^{sd} = \frac{\alpha}{2} \sum_n \zeta_n \cdot \zeta_{k+n} \cdot e^{j(\varphi_{k+n} - \varphi_n)} \quad (35)$$

and

$$S(k) \cdot (\Delta k)^2 = E\{\zeta_k^{sd}(\zeta_k^{sd})^*\} = \frac{\alpha^2}{4} \sum_n E\{(\zeta_n \cdot \zeta_{k+n})^2\} \quad (36)$$

Consequently,  $\zeta_k^{sd}$  and  $\zeta_k^{sc}$  are complex values. Because by quadratic filtering, the same energy is spread over the long and short waves, and also because the short wavelength spectrum bandwidth is smaller than the long frequency spectrum bandwidth, the short frequency magnitude is lower than the long frequency magnitude, as



can be seen in fig. 8. The nonlinear image bispectrum shows several phenomena which can be divided into two classes: the primary phase coherency phenomena and the secondary ones.

### The Primary Phase Coherency Phenomena

(PPCP) are only those phenomena implying a phase coupling between two waves and a third wave being generated by the interaction of the first two waves. Such a phenomenon occurs for:

$$B(L, M) B(M, M) B(S, M)$$

Where  $L$  denotes a wave included in the long wave spectrum (31),  $S$  is a wave included in the short wave spectrum (32) and  $M$  is an original wave spectrum (30). For instance, in the first case, the bispectrum is equal to:

$$\begin{aligned} B(k_1, k_2).(\Delta k)^3 &= \frac{\alpha}{2} E\{\zeta_{k_1}.e^{j\cdot\varphi_{k_1}}.\zeta_{k_2}.e^{j\cdot\varphi_{k_2}}.(\zeta_{k_1+k_2}^{sd})^*\} \\ &= \frac{\alpha}{2} E\{(\zeta_{k_1}.\zeta_{k_2})^2\} \end{aligned} \quad (37)$$

and then, assuming that  $C = 0$ , for an ideal infinite number of trials:

$$P(k_1, k_2) = \sqrt{\frac{E\{\zeta_{k_1}.\zeta_{k_2}\}}{\sum_n E\{(\zeta_n.\zeta_{k_1+n})^2\}}} \quad (38)$$

In this case we must notice that

$$T_{RA}(k_1) = \sum_{k_2} P^2(k_1, k_2) = 1 \quad (39)$$

and the coefficient  $\alpha$  does not interfere in the bicoherence calculation.

### The Secondary Phase Coherency Phenomena

(SPCP) occur between waves not bound by a quadratic interaction. These phenomena can be found for:

$$B(S, S), B(L, S), B(L, L)$$

In each of these three cases, the waves have not interacted or have not been generated by interactions of the other two waves, but by considering:

$$\zeta_{k_1}^{sc} . (\zeta_{k_2}^{sc})^* = \frac{\alpha^2}{4} \sum_n \sum_{n'} \zeta_n . \zeta_{n'} . \zeta_{k_1-n} . \zeta_{k_2-n'} . e^{j\varphi} \quad (40)$$

with

$$\varphi = \varphi_n - \varphi_{n'} + \varphi_{k_1-n} - \varphi_{k_2-n'} \quad (41)$$

Assuming that  $n = n'$  then  $\varphi = \varphi_{k_1-n} - \varphi_{k_2-n}$ . But  $(k_1 - n) \in M$  and  $(k_2 - n) \in M$ , so these waves have destructively interacted at the frequency  $k_1 - k_2$  and

consequently the phase of a term of the sum is equal to  $\varphi_{k_1-n} - \varphi_{k_2-n}$  (see (35)). Then

$$\begin{aligned} B(k_1 - k_2, k_1).(\Delta k)^3 &= E\{\zeta_{k_1-k_2}^{sd} . \zeta_{k_1}^{sc} . (\zeta_{k_2}^{sc})^*\} = \\ &= \frac{\alpha^3}{8} \sum_n E\{(\zeta_n . \zeta_{k_1-n} . \zeta_{k_2-n})^2\} \end{aligned} \quad (42)$$

and, assuming an ideal case (an infinite number of realisations) then  $P^2(k_1 - k_2, k_1) = \frac{A}{B}$  with

$$A = \sum_n \sum_{n'} E\{(\zeta_n . \zeta_{k_1-n} . \zeta_{k_2-n})^2\} E\{(\zeta_{n'} . \zeta_{k_1-n'} . \zeta_{k_2-n'})^2\} \quad (43)$$

$$\begin{aligned} B &= \sum_n \sum_{n'} \sum_{n''} (E\{(\zeta_n . \zeta_{k_1-n})^2\} . E\{(\zeta_{n'} . \zeta_{k_2-n'})^2\} . \\ &E\{\zeta_{n''} . \zeta_{k_1-k_2+n''}\}^2) \end{aligned} \quad (44)$$

Unfortunately this bicoherence expression does not give a simple result in the BTs. This kind of phase coupling occurs in the first and second cases  $B(S, S)$ ,  $B(L, S)$ , and does not imply original spectrum wave. Thus, if the original spectrum has been totally removed, nonlinearity detection would be still possible by these phenomena. The third SPCP is similar, and by considering :

$$\zeta_{k_1}^{sd} . (\zeta_{k_2}^{sd})^* = \frac{\alpha^2}{4} \sum_n \sum_{n'} \zeta_n . \zeta_{n'} . \zeta_{k_1+n} . \zeta_{k_2+n'} . e^{j\varphi} \quad (45)$$

with

$$\varphi = -\varphi_n + \varphi_{n'} + \varphi_{k_1+n} - \varphi_{k_2+n'} \quad (46)$$

assuming that  $n = n'$ , then  $\varphi = \varphi_{k_1+n} - \varphi_{k_2+n}$ . But  $k_1 + n \in M$ ,  $k_2 + n \in M$ , so these waves have destructively interacted at  $k_2 - k_1$  so

$$\begin{aligned} B(k_2 - k_1, k_1).(\Delta k)^3 &= E\{\zeta_{k_2-k_1}^{sd} . \zeta_{k_1}^{sd} . (\zeta_{k_2}^{sd})^*\} = \\ &= \frac{\alpha^3}{8} \sum_n E\{(\zeta_n . \zeta_{k_1+n} . \zeta_{k_2+n})^2\} \end{aligned} \quad (47)$$

Thus, if the original spectrum has been totally removed, nonlinearity detection would be still possible by these phenomena. The third SPCP is similar and by considering :

$$\zeta_{k_1}^{sd} . (\zeta_{k_2}^{sd})^* = \frac{\alpha^2}{4} \sum_n \sum_{n'} \zeta_n . \zeta_{n'} . \zeta_{k_1+n} . \zeta_{k_2+n'} . e^{j\varphi} \quad (48)$$

with

$$\varphi = -\varphi_n + \varphi_{n'} + \varphi_{k_1+n} - \varphi_{k_2+n'} \quad (49)$$

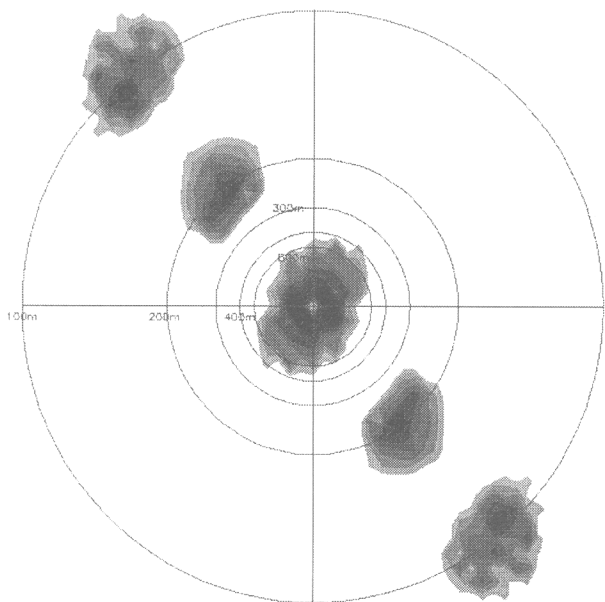


Fig. 9. Range-Azimuth Table

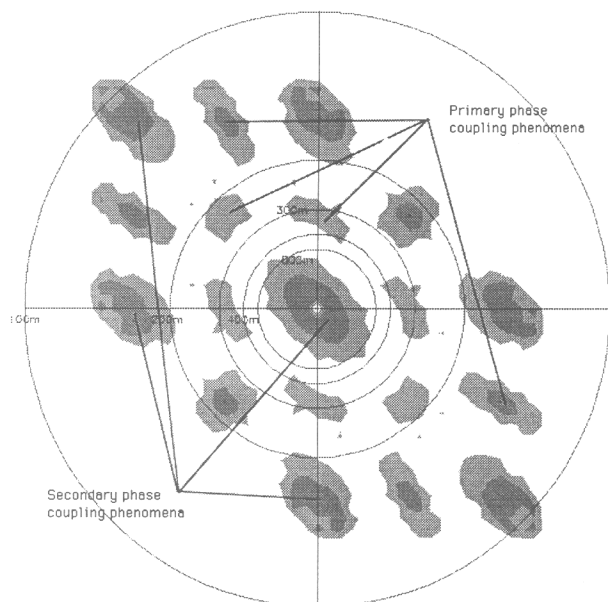


Fig. 11. Range-Range Table

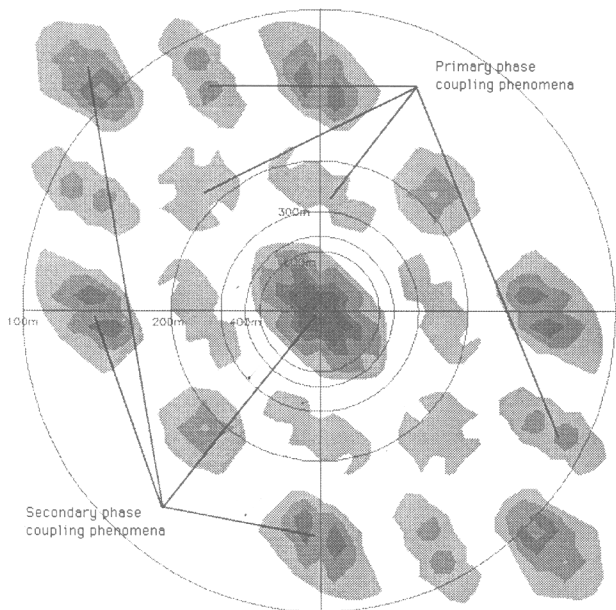


Fig. 10. Azimuth-Azimuth Table

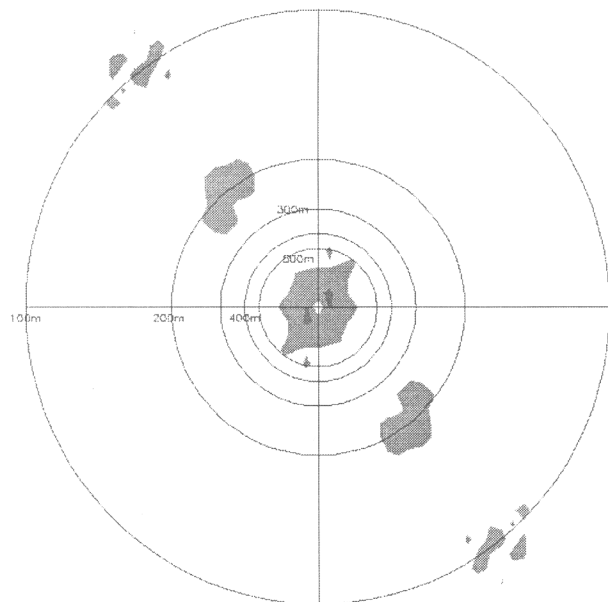


Fig. 12. "Linear" signal RA Table

Assuming that  $n = n'$ , then  $\varphi = \varphi_{k_1+n} - \varphi_{k_2+n}$ . But  $k_1 + n \in M$ ,  $k_2 + n \in M$ , so these waves have destructively interacted at  $k_2 - k_1$  so

$$B(k_2 - k_1, k_1) \cdot (\Delta k)^3 = E\{\zeta_{k_2-k_1}^{sd} \cdot \zeta_{k_1}^{sd} (\zeta_{k_2}^{sd})^*\} = \frac{\alpha^3}{8} \sum_n E\{(\zeta_n \cdot \zeta_{k_1+n} \cdot \zeta_{k_2+n})^2\} \quad (50)$$

and  $P^2(k_2 - k_1, k_1) = \frac{A}{B}$

$$A = \sum_n \sum_{n'} E\{(\zeta_n \cdot \zeta_{k_1+n} \cdot \zeta_{k_2+n})^2\} \cdot E\{(\zeta_{n'} \cdot \zeta_{k_1+n'} \cdot \zeta_{k_2+n'})^2\} \quad (51)$$

$$B = \sum_n \sum_{n'} \sum_{n''} E\{(\zeta_n \cdot \zeta_{k_1+n})^2\} \cdot E\{(\zeta_{n'} \cdot \zeta_{k_2+n'})^2\} \cdot E\{(\zeta_{n''} \cdot \zeta_{k_2-k_1+n''})^2\} \quad (52)$$

As the previous phenomenon, this one does not imply the original wave spectrum, and would occur even if waves from the original spectrum were missing. In order to verify our theory we computed the three BTs for the nonlinear signal. On the RA table (fig. 9) all spectrum frequencies give a non null bicoherence, for the reason that they have all interacted in the nonlinear process. This table must not be confused with the spectrum as is seen in the following subsection. In the AA and RR tables (fig. 10-11), primary and secondary phase coupling phenomena are clearly separated, the secondary ones being the strongest. In order to compare "linear" and "nonlinear" signals, we computed the BTs for a signal having the same spectrum as the nonlinear signal (random phases have been added to the squared signal for each realisation). The RA table for the "linear" signal (fig. 12) is much smaller than the "nonlinear" one (fig. 9) and the separation between both signals can easily be made. The next section is devoted to the study of BT behaviour in the case of partial filtering of the original or of the squared signal.

### Third example: Filtered "nonlinear" signal

The first example is to verify the SPCP existence. So we totally removed the original spectrum and only the phase coupling between short and long waves is possible. The RA table has the same order of magnitude as the complete "nonlinear" signal RA table (fig. 9, fig. 12 and fig. 13 are represented with the same grey level scale), thus proving that these phenomena exist and are very strong. The RR and AA tables (not shown in this paper) are composed only of SPCP present in fig. 10-11. In order to verify that the RA table and the spectrum can contain very different patterns,  $H_2(k)$  (see fig. 3) was designed in order to have a very narrow pass-band (consequently few waves interact). The spectrum (fig.

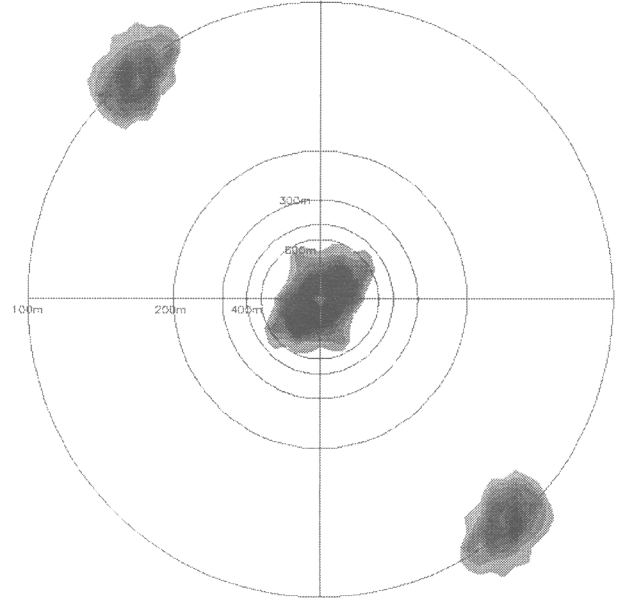


**Fig. 13.** Range-Azimuth Table of the "nonlinear" signal without original spectrum

14) is composed of three parts, the large original spectrum and two narrow and weaker spectra generated by interactions. The RA table (fig. 14) contains three equal parts, having the same order of magnitude (because the BTs measure the amount of nonlinearity which is equal for waves created by interaction or having interacted) and the same bandwidth (the waves which have not interacted being removed). In the SAR imaging process, nonlinearities are assumed to be oriented along the azimuth axis. To simulate such behaviour, the squared signal was filtered with a 2D directional filter (an all-pass filter along one axis and a low-pass filter, with a very low cut-off frequency  $k_{co}$ , along the other axis). The spectrum is shown in fig. 15. If the waves travel along the nonlinear axis ( $90^\circ$  from the horizontal axis), then the linear axis table (RR in this case) contains a strong peak around the continuous component whereas the nonlinear axis table is almost null (fig. 16). This pattern is easily explained because the bicoherence is high for  $(k_x, k_y) \in [-0.5, 0.5] \times [-k_{co}, k_{co}]$ . It is then logical that the summation of the squared bicoherence over  $k_y$  ( $k_x$  fixed) is higher than for a summation over  $k_x$ . When the waves travel far from the nonlinear axis then BTs are almost null (only estimation errors provide non null values). From this example we may conclude that when there are a linear axis and a nonlinear one, the stronger bicoherence values are located near the continuous component of the linear axis table. The BTs constitute a useful tool to analyse the nonlinearity contained in a 2D signal. Their application is

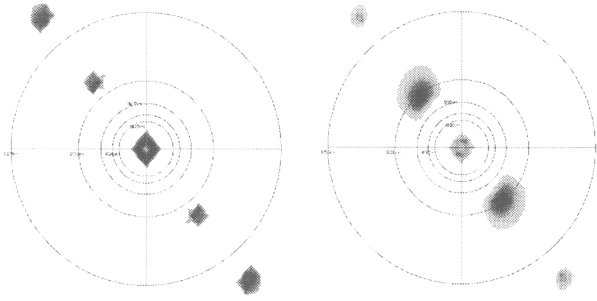


Fig. 14. Filtered signal RA table (left) and spectrum (right)

not easy, but they allow the information contained in the 4D bicoherence to be summarised. The main bicoherence disadvantage is its strong dependence on the number of realisations, and its estimation can provide a rather high amount of nonlinearity even when there is no phase coupling in the signal. In the second subsection, BTs obtained on SAR images are analysed.

5.2 ERS-1 SAR images

The validity of the quadratic approximation has been already tested for several nonlinear models. For instance a monochromatic signal of pulsation  $\omega$  passing through an exponential system generates "spurious" components at  $0, 2\omega, 3\omega, \dots$ , and the magnitudes of these components are asymptotically equal, even if component  $\omega$  remains the strongest after the continuous component (Garello and Le Caillec, 1996). The nonlinear mapping SAR process has also been decomposed into a Second Order Volterra Model and first results are related in (Le Caillec et al., 1996). These results show, for realistic significant wave heights of the sea surface, rather good agreement between the spectrum and the BTs of a complete nonlinear SAR process and the spectrum and the BTs of the quadratic approximation of this process. We present here the results for five typical images, the characteristics of which can be found in table 1 (Day, hour latitude, longitude, estimated dominant wavelength in meters **DW**, estimated azimuth cut-off in meters **ACO**,

Nbr	1	2	3	4	5
Day	6 Oct. 93	8 Oct. 93	5 Oct. 93	2 Oct. 93	30 Sep. 93
Hour	23:39:36	13:15:26	0:41:02	0:43:50	23:35:27
Lat.	24.72	3.09	18.34	48.51	50.62
Long.	341.18	316.85	326.81	320.32	336.80
DW	345	294	101	94	227
ACO	221	142	232	317.5	413
Max.	17.7	62.7	77.8	75.3	6.4

Table 1. Image data

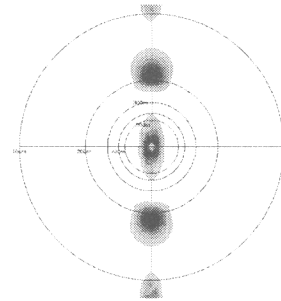


Fig. 15. Directionally filtered signal spectrum

BT maximum value **Max.**)

Image 1 (fig. 18) This image contains a dominant wave travelling in the azimuth direction. The RA table and the spectrum are similar and the BT maximum value is rather low (see table 1). The AA table shows a pattern made up of two sets of symmetric peaks, located respectively at  $(0, M)$  and  $(M, M)$ . The pattern, except for secondary phase coupling phenomena, is a similar pattern to the one in fig 10-11. By considering all  $\sqrt{S(k_1).S(k_2).S(k_1 + k_2)}$  greater than 2%, the secondary phase coupling phenomena does not appear but lines along  $2\pi/k_x^{1,2} \simeq 400m$  (and its symmetric lines) appear in the AA table and  $2\pi/k_y^{1,2} \simeq 0m$  (and its symmetric lines) appear in the RR table (see fig 18). But these lines are due only to the fact that the highest frequency components are located about these wavelengths and that we deal with a finite number of realisations. However, a more accurate study of the bicoherence shows high bicoherence values for spectrum components about 350 m. The nonlinear interactions would occur for wave components about 170 m. These components have been removed by the azimuth cut-off. For this reason, nonlinearity detection for "constructive" interactions remains difficult. However, because of the lack of destructive interactions and SPCP, we can conclude that this image does not contain classical quadratic interactions produced by a Second Order Volterra Model. The lack of nonlinearity can be partially explained by the fact that the short waves, which would have been generated by interactions, have been removed by the azimuth cut-off and the long waves by a high pass filter inherent to quadratic interactions (Le Caillec et al., 1996).

Image 2 (fig. 19) In this image, there are no great differences between the RA table and the spectrum either. Only some small parts are darker, and especially a peak around 500m in the azimuth direction (by taking into account all the triple product values greater than 2% this peak becomes stronger than the one about 300m). A study of the bicoherence shows unusually high nonlinearity rates, especially between the waves about 500m, proving the existence of a nonlinear phenomenon for

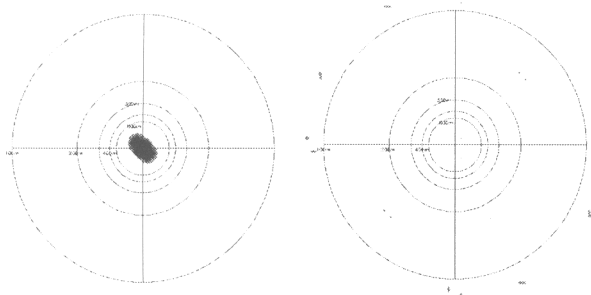


Fig. 16. Directionally filtered RR (left) and AA (right) tables

these waves.

Image 3 (fig. 20) The relevant information is that the RA table and the spectrum are different. In particular, the waves travelling in the azimuth direction have a greater bicoherence whereas those travelling in the range show few interactions, even for a bicoherence computation over the whole support. Consequently, only one of the two dominant wave sets has interacted, which is the one that propagates in the azimuth direction. The other relevant information is:

-Firstly, the components which have interacted less are those with  $2\pi/k_x^{1,2} = 0$  (i.e. along the range axis), whereas those having the same projection onto the azimuth axis ( $k_x^1 = k_x^2$ ) have the strongest interactions. This observation agrees with the classical velocity bunching theory which states that a linear phenomenon is provided when waves travel in the range direction.

-Secondly, the AA table is stronger than the RR one, especially for long waves, proving that the azimuth axis is more relevant than the other in the nonlinear process.

Image 4 (fig. 21) The conclusions are similar to those of the previous image, but the computed difference of the amount of nonlinearity between the two wave sets is smaller, perhaps because the wave magnitude in the azimuth direction is lower.

Image 5 (fig. 22) Few nonlinear interactions are detected, but these BTs show similar patterns as those contained for the BTs of fig. 22. However waves with such a long crest line are not observed in the open sea. The mapping mechanism of this image is not easy to understand and seems to be nonlinear. The lack of nonlinearity detection is perhaps due to blurring of higher order nonlinearities.

In order to summarise the information collected from these images we can conclude that, even if the dominant wavelength is near the range axis, quadratic nonlinearities can occur (images 3,4). Whereas when the waves propagate in the azimuth direction, the image does not contain any apparent quadratic nonlinearity (image 1-2), thus proving that the quadratic approximation is not suitable in this case for the complete nonlinear SAR

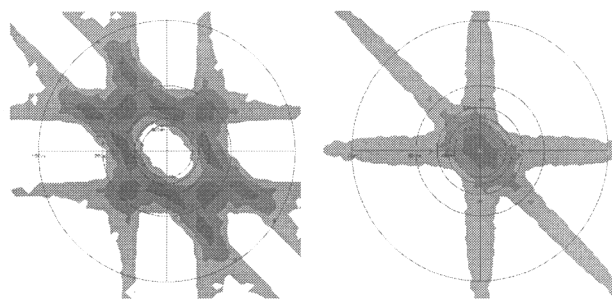


Fig. 17. Image 1 AA table (left) and RR table (right)

process. Also, it has been established that the strongest interactions occur for waves having the same azimuth wavenumber projection, whilst the components near the range axis interact the least. The frequencies with the highest amount of phase coupling have a wavelength between 200-300 meters. The SAR mapping (leading to the SAR spectrum of (6)) decomposition on a Second Order Volterra Model given in Le Caillec et al. (1996), shows that the quadratic interactions are both low-pass and high-pass filtered. The low pass filtering is the well-known azimuth cut-off which acts on nonlinear and linear components, but the quadratic waves are also high-pass filtered, because by expanding the exponential in (5) the quadratic interactions are multiplied by  $k_x$ . This implies that these interactions (but also higher order nonlinear interactions) are removed near the range axis as observed for image 3-4. Consequently, quadratic interactions can only be found in an azimuth frequency band around 300m (as noticed for image 3-4). Moreover "destructive" quadratic interactions can be located in this band only if the original spectrum is close to the range axis. The waves  $(k_x, k_y)$  and  $(-k_x, k_y)$ , assuming that  $k_x$  is fairly small, have significant frequency components and their "destructive" interactions are located at  $(-2.k_x, 0)$ , and these interactions are consequently in the frequency band where quadratic nonlinearities are not filtered. "Constructive" interactions have too high wavelengths to be detected. However due to the weakness of the nonlinear components in this case, the assumption of a linear system when the waves travel in the range direction is a good approximation. In other cases, where the original sea surface spectrum is not close to the range axis, both constructive and destructive interactions are removed (respectively by the high pass filtering inherent to the quadratic interactions and by the azimuth smearing). For this reason, images where the dominant waves are in the azimuth direction contain few quadratic interactions. However two remarks must be formulated:

-The first one is that, if the significant wave height (and consequently the displacement) becomes too high, the original spectrum can be removed (by the azimuth

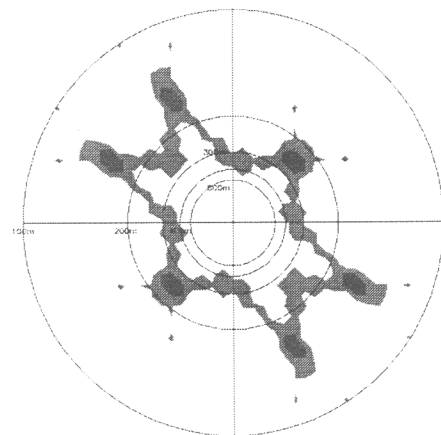
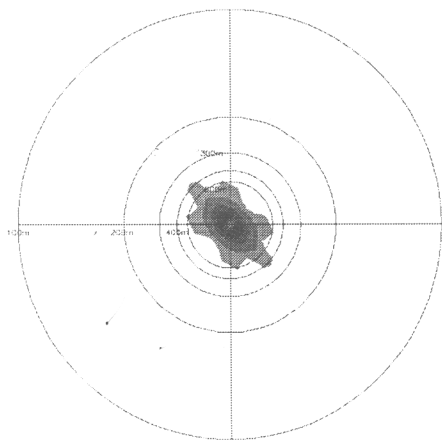
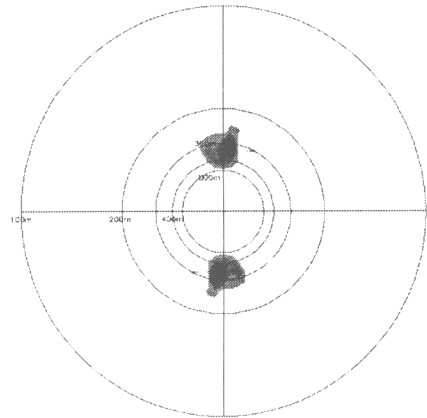
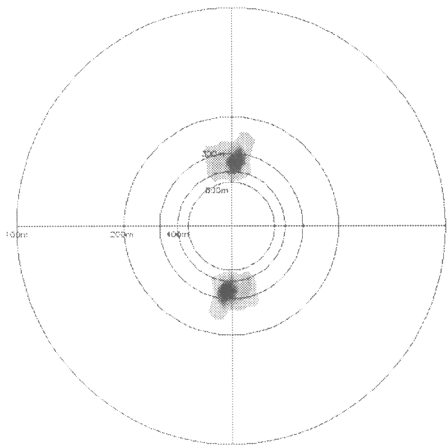
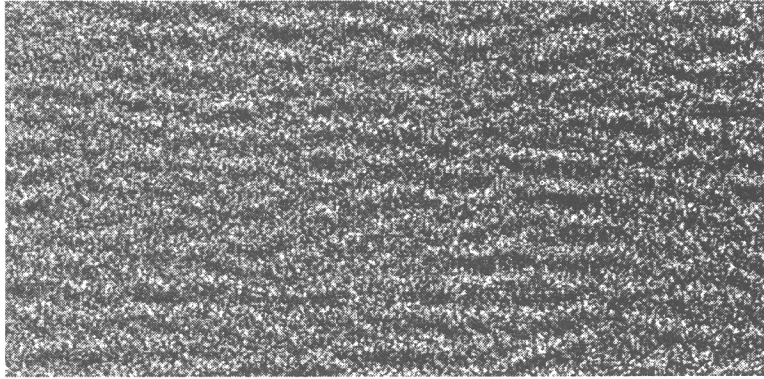


Fig. 18. Image 1, spectrum (upper left), RA table (upper right), RR table (lower left), AA table (lower right)

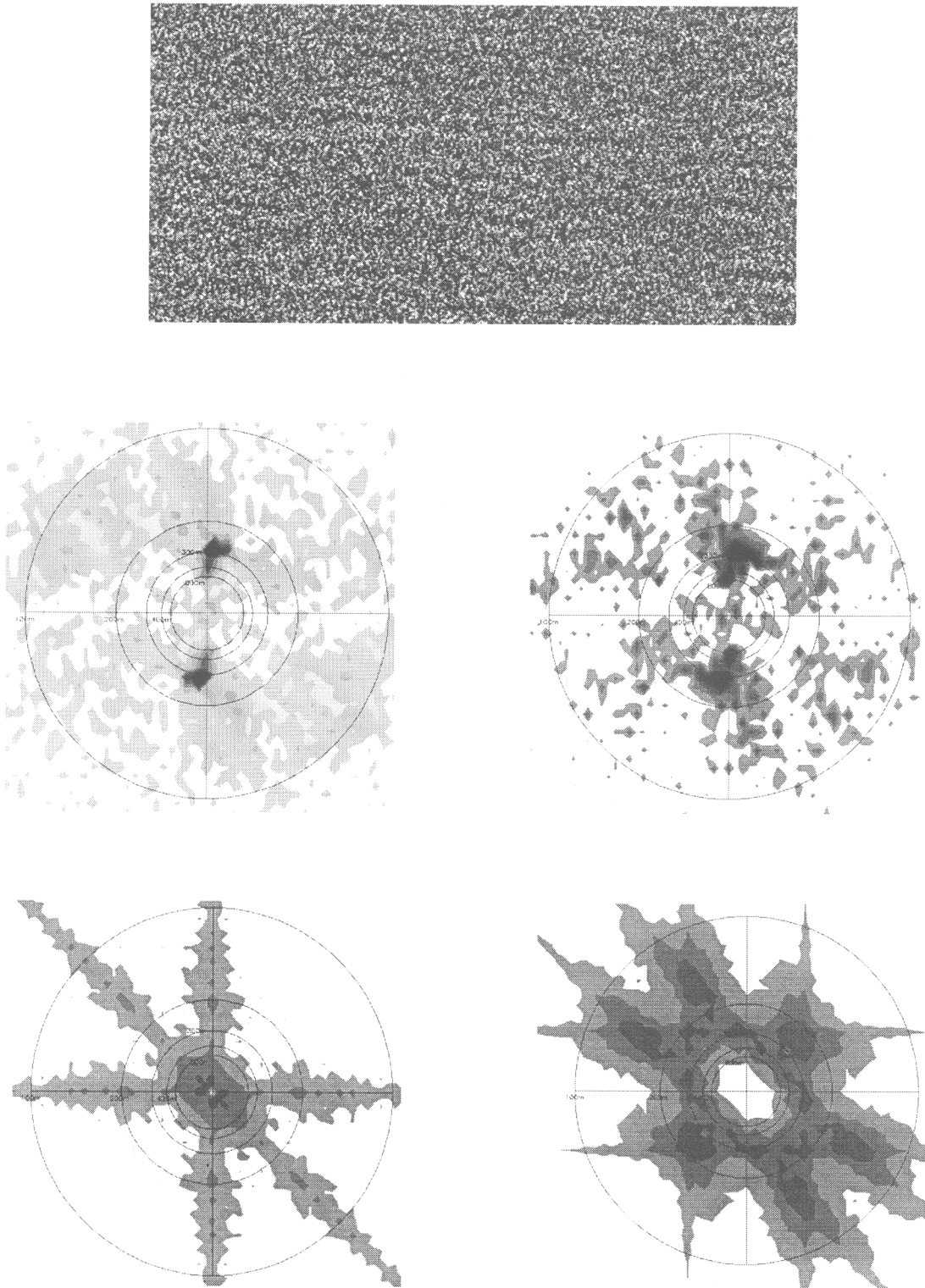


Fig. 19. Image 2, spectrum (upper left), RA table (upper right), RR table (lower left), AA table (lower right)

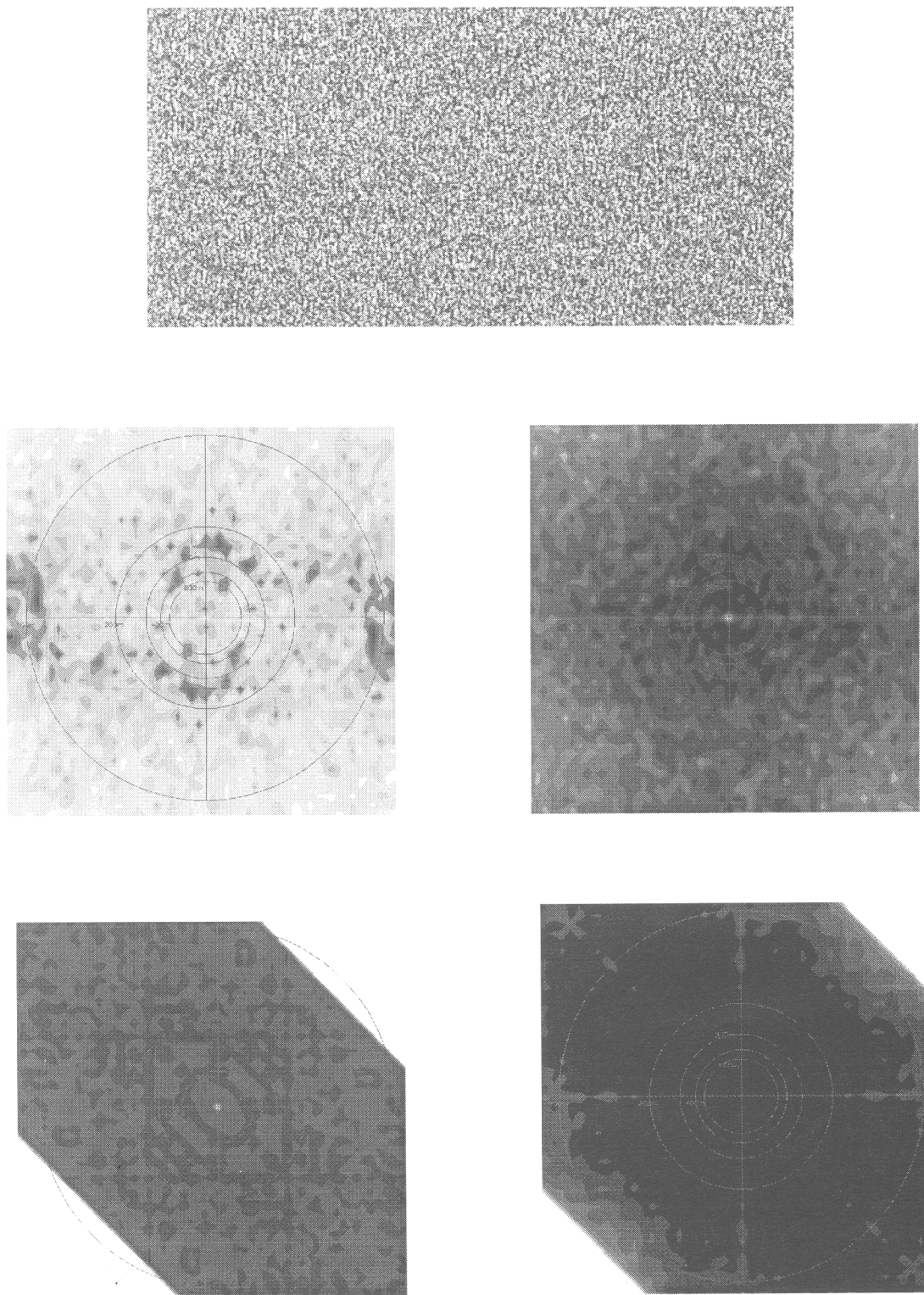


Fig. 20. Image 3, spectrum (upper left), RA table (upper right), RR table (lower left), AA table (lower right)



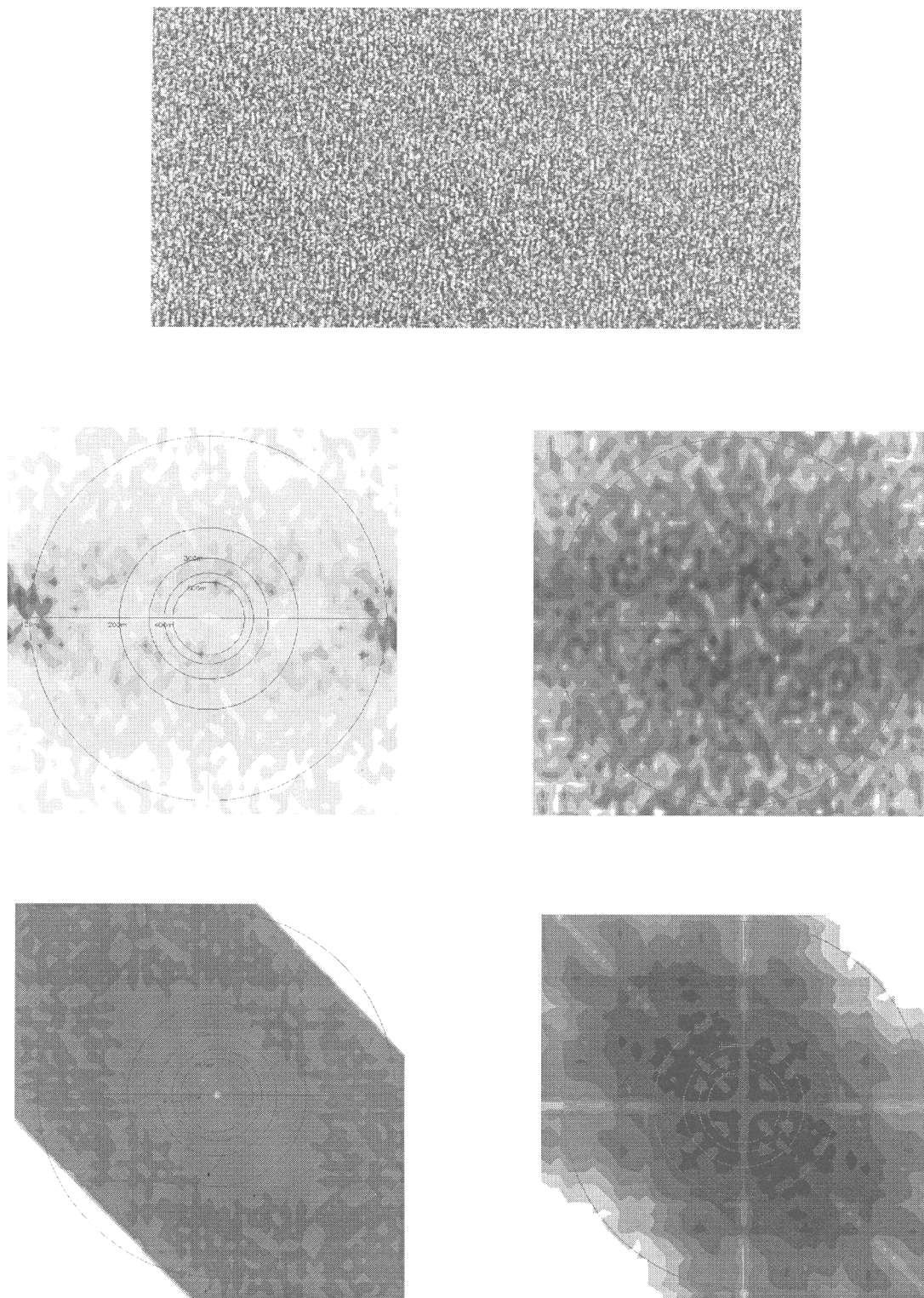


Fig. 21. Image 4, spectrum (upper left), RA table (upper right), RR table (lower left), AA table (lower right)

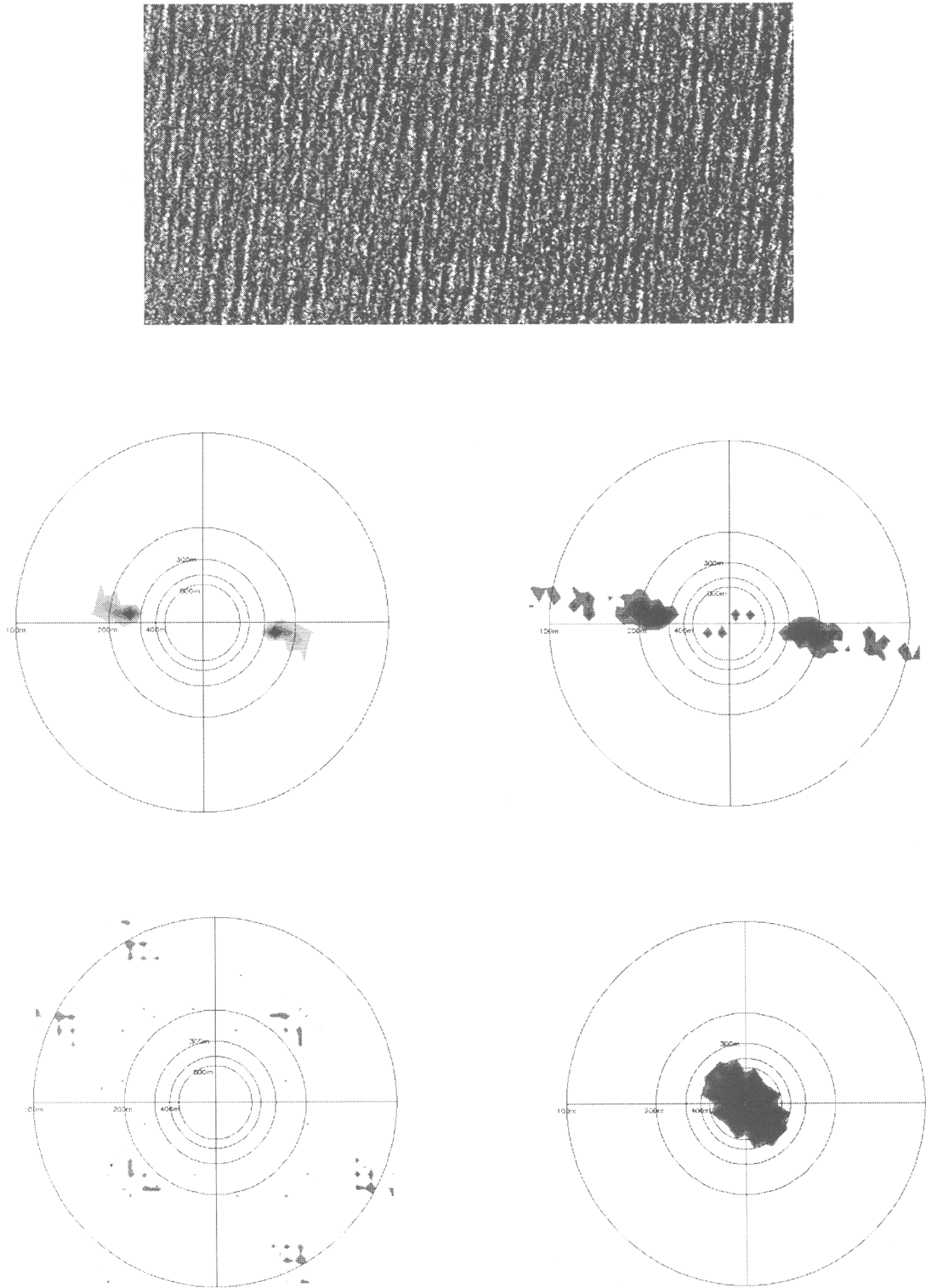


Fig. 22. Image 5, spectrum (upper left), RA table (upper right), RR table (lower left), AA table (lower right)

smearing) and the destructive interaction frequency components can exceed those of the original filtered sea surface spectrum. The resulting SAR spectrum is located near the range axis (Bruning found such results in Bruning et al. (1990)).

-Secondly, our method seems to fail in an apparently nonlinear case (image 5), without any convincing explanation. Consequently the mechanism leading to the Fourier coefficient expression of (5) and to the spectrum of (6) agrees with results found both on real and simulated SAR images, but a mechanism such as that of fig 22, remains to be analysed.

## 6 Conclusion

In this paper, we have presented a way to detect nonlinearities or at least their quadratic approximation for 2D signals and more specifically for SAR images of the ocean surface. For that purpose we have shown that HOS methods were very powerful tools and we have developed one of the possible bispectrum (or bicoherence) estimations in order to analyse the images. We have particularly put the emphasis on the quantification of the amount of nonlinearity present at given frequencies on the images and introduced the bicoherence standard deviation and bicoherence tables in order to visualise and synthesise the information contained in a 4D form. This latter tool is very well adapted for the detection and localisation of nonlinearities as was shown in our simulation using a 2D Second Order Volterra Model.

Besides, the tables of bicoherence are particularly interesting if used in the context of SAR images, i.e. for 2D signals that are naturally divided along two preferred axes (range and azimuth). We were then able to detect the amount of nonlinearity provided by the coupling of frequencies in either the range or the azimuth directions or between these two directions. For instance, the Range-Azimuth table provides a fast localisation of the nonlinearity interactions and a possible estimation of their strength when compared to the image spectrum. We demonstrated on the simulations that it was not only possible to detect frequencies created by nonlinear interactions between two waves present on the input spectrum (and referred to Primary Phase Coherence Phenomena, PPCP), but furthermore, that we were able to detect the existence of a second level of phase coupling (referred as Secondary Phase Coherence Phenomena, SPCP) between waves having no nonlinear interactions in the original (input) spectrum. Indeed we noted the appearance of frequencies generated at the first level (PPCP), i.e. by waves existing in the input spectrum, and presenting a strong amount of phase coupling giving rise to another level (SPCP) of nonlinearities between them.

The SPCP are very relevant due to the fact that they allow a possible discrimination between the two cases where i) the bicoherence estimation yields a non zero result due to the finite number of realisations used and ii) a nonlinear phenomenon is present but weak.

This is the first time that such a phenomenon is predicted and observed on simulations. In Le Caillec et al. (1996) we have shown that on real SAR images these nonlinearities are constrained by different filtering effects (azimuth cut-off, ...), implying that the mechanisms developed for setting equation (6) is correct. Nevertheless equation (6) does not contain information on the localisation and on the strength of the nonlinearities which can be only obtained by using Higher Order Spectra. We have especially shown that nonlinearities occur mainly when the waves travel in the range direction, but they generate rather weak components, and that the interactions are filtered for other wave propagation directions. Higher Order Spectra (and the BTs which are the more complete version for 2D signals) are powerful tools for dealing with nonlinear signals and systems, but they have two main limitations.

- Firstly, the limited and generally small number of realisations can induce false nonlinearity detection or avoid it if the "nonlinear" component bicoherence amount is too weak and consequently blurred into a misestimated amount of bicoherence. By using the statistics of a modified bicoherence (and more especially the tail of the distribution), we can detect phase coupling with few or non independent realisations (Garello and Le Caillec, 1996). The independence of the subsets of the ERS-1 images has been verified by a similar method (Garello and Le Caillec, 1996).

- Secondly, classical phase coupling detection can fail for non passive systems. For instance, if the signal of (12) is shifted in frequency by  $\delta k$ , then classical phase coupling detection using the bispectrum does not work for the triplet  $k_1 + \delta k, k_2 + \delta k, k_1 + k_2 + \delta k$ . A solution, using the Third Order Wigner-Ville Transform, to detect shifted phase coupling, is provided in Le Caillec and Garello (1996). As previously mentioned, even if all results are not easy to explain, SAR simulations which are presently underway will help understand the working of the SAR image process and of its second order approximation. Moreover, it will be possible in our future work to include the trispectrum in order to take into account cubic nonlinearities. Even if using the bispectrum cannot always provide definitive answers, due to its capacity to separate the coherent backscattering (wave modulation) from the incoherent one (speckle noise), it remains a prospective tool for removing noise.

*Acknowledgement.* Special thanks to Vincent Kerbaol and Tanos El Fouhaily, for their help during this work, to Janet Omrod and Robert "Bobus" Fiset for their advice on the writing of this paper. This work was granted by the IFREMER contracts

N° 93-2-422-038/DROS-OS

N° 93-2-422-101/DROS-OS

N° 93-2-422-057/DROS-OS

and partially supported by the european MAST III programme of EC under the contract

N° MAS3-CT95-0027

## References

- Alpers, W. and Bruning, C., On the relative importance of motion-related contributions to the SAR imaging mechanism of ocean surface wave, *IEEE trans. on Geoscience and Remote Sensing, GE-24*, 873-885, 1986.
- Alpers, W., Duncan, B., and Ruffenach, C., On the detectability of ocean surface waves by real and synthetic aperture radar, *J. Geophys. Res.*, 86, 6481-6498, 1981.

- Bruning, C., Alpers, W., Zambreski, L., and Tilley, D., Validation of a synthetic aperture radar ocean wave imaging theory by the shuttle imaging radar-b experiment over the north sea, *J. Geophys. Res.*, *93*, 15403-15425, 1988.
- Bruning, C., Alpers, W., and Hasselmann, K., Monte-carlo simulation studies of the nonlinear imaging of a two dimensional surface wave field by a synthetic aperture radar, *Int. J. of Remote Sensing*, *11*, 1697-1727, 1990.
- Chandran, V. and Elgar, S., Bispectral analysis of two-dimensional random processes, *IEEE Trans. on ASSP*, *ASSP-38*, 2181-2186, 1990.
- Erdem, A. and Tekalp, A., New theoretical results on the bistatistics of 2d signals, *Higher Order Statistics*, J.L. Lacoume (Editor). Elsevier Publisher., 99-102, 1992.
- Garello, R. and Le Caillec, J.M., Etude des methodes spectrales d'ordre supérieur: le bispectre des images SAR, *IFREMER-ENSTB, internal report*, 1996.
- Giannakis, G. and Mendel, J., Cumulant-based order determination of non-gaussian arma models, *IEEE Trans. on ASSP*, *ASSP-38*, 1411-1423, 1990.
- Giannakis, G. and Swami, A., On estimating noncausal nonminimum phase arma models of non gaussian processes, *IEEE Trans. on ASSP*, *ASSP-38*, 478-475, 1988.
- Hara, T. and Plant, W., Hydrodynamic modulation of short wind-wave spectra by long waves and its measurement using microwave backscatter, *J. Geophys. Res.*, *99*, 9767-9784, 1994.
- Hasselmann, K. and Hasselmann, S., On the non linear mapping of an ocean wave spectrum into a synthetic aperture radar image spectrum and its inversion, *J. Geophys. Res.*, *96*, 10713-10729, 1991.
- Hasselmann, K., Raney, R., W.J. Plant, W. A., Schuman, R., Lyzenga, D., Rufenach, C., and Tucker, M., Theory of synthetic aperture radar ocean imaging: A marsen view, *J. Geophys. Res.*, *90*, 4659-4686, 1985.
- Keller, W. and Wright, J., Microwave scattering and the straining of wind generated waves, *Radio Science*, *10*, 139-147, 1975.
- Kim, K. and Powers, E., A digital method of modeling quadratically nonlinear systems with a general random input, *IEEE Trans. on ASSP*, *ASSP-36*, 1758-1769, 1988.
- Kim, Y. and Powers, E., Digital bispectral analysis and its application to nonlinear wave interactions, *IEEE trans. on plasma science*, *PS-7*, 120-131, 1979.
- Krogstad, H., A simple derivation of Hasselmann's nonlinear ocean-synthetic aperture radar transform, *J. Geophys. Res.*, *97*, 2421-2425, 1992.
- Krogstad, H., Samset, O., and Vachon, P., Generalization of the non-linear ocean-SAR transform and a simplified SAR inversion algorithm, *Atmosphere-Ocean*, *32*, 61-82, 1994.
- Le Caillec, J.M. and Garello, R., Detection and quantification of nonlinearities in a modified volterra model by using wigner-ville higher order transform, *Proc. of International Symposium on Time-Frequency and Time-Scale Analysis*, 181-184, 1996.
- Le Caillec, J.M., Garello, R., and Chapron, B., Detection of nonlinearities in sea surface imaging process using bispectrum method estimation, *Proc. of ICASSP*, *3*, 1585-1588, 1995.
- Le Caillec, J.M., Garello, R., and Chapron, B., Study of the second order approximation of the velocity bunching in the SAR image process using the bispectrum, *Proc. of IGARSS*, *1*, 612-614, 1996.
- Mastin, G., Watterberg, P., and Mareda, J., Fourier synthesis of ocean scenes, *IEEE Trans. on Computer Graphics and Applications*, 16-23, 1987.
- Nikias, C. and Mendel, J., Signal processing with higher-order spectra, *IEEE Signal Magazine*, 10-37, 1993.
- Nikias, C. and Petropulu, A., *Higher-Order Spectra Analysis - a nonlinear signal processing framework*, PTR Prentice Hall, Englewood Cliffs, NJ, 1993.
- Nikias, C. and Raghuvver, M., Bispectrum estimation: A digital signal processing framework, *Proceedings IEEE*, *75*, 869-891, 1987.
- Raghuvver, M., Time-domain approaches to quadratic phase coupling estimation, *IEEE Trans. on Automatic Control*, *35*, 48-56, 1990.
- Raghuvver, M. and Nikias, C., Bispectrum estimation: A parametric approach, *IEEE Trans. on ASSP*, *ASSP-33*, 1213-1230, 1985.
- Schetzen, M., *The Volterra and Wiener theories of nonlinear systems*, Wiley J., New York, 1980.